

Modelling of a multiphase reacting turbulent jet: Application to supersonic carbon injection in siderurgic furnaces

Marina Campolo^{a,*}, Michele Andreoli^a, Leonardo Tognotti^b, Alfredo Soldati^{a,c,d}

^aCentro Interdipartimentale di Fluidodinamica e Idraulica, Università di Udine, 33100 Udine, Italy

^bDipartimento di Ingegneria Chimica, chimica industriale e scienza dei materiali, Università di Pisa, 56126 Pisa, Italy

^cDipartimento di Energetica e Macchine, Università di Udine, 33100 Udine, Italy

^dDepartment of Fluid Mechanics, CISM – Centro Internazionale di Scienze Meccaniche, 33100 Udine, Italy

Received 20 October 2006; received in revised form 4 April 2007; accepted 11 May 2007

Available online 24 May 2007

Abstract

In this work, we present an original numerical approach developed to evaluate injection performances of a new injection system (More s.r.l.[®]) designed for siderurgic applications. The system exploits a supersonic jet of oxygen to inject carbon particles into the slag. A precise characterization of the injection process by experimental analysis is extremely difficult and costly because of the complex chemico-physical mechanisms controlling transport, burn-out and devolatilization of carbon particles inside the oxidizing, high temperature environment of the electric arc furnace. In this work, we use numerical simulations to test and characterize injector performances for conditions corresponding to a 120 ton capacity electric furnace. We exploit the best available, state of the art numerical techniques to characterize the fluid-dynamics and chemico-thermal environment seen by carbon particles, which we couple to *ad hoc* research tools (Lagrangian tracking routines and complex chemistry schemes) to reproduce carbon consumption due to thermally and chemically controlled kinetics. These data are used to analyse the factors controlling injector performances, to identify a most critical configuration of the injector in the furnace and to obtain a conservative estimate of the injection yield of carbon particles. The performances of the injection device are evaluated in two different geometries and for three different types of carbon particles. Numerical results confirm that the supersonic injection promotes high injection yields: (i) by decreasing drastically the residence time of carbon particles inside the furnace and (ii) by modifying the hot reacting environment seen by carbon particles. © 2007 Elsevier Ltd. All rights reserved.

Keywords: Particle injection; Supersonic jet; Reactor network analysis

1. Introduction

Multiphase reacting jets are widely used in industrial applications (from fuel burners to spray driers, to cite a few) and often represent critical steps in the industrial process, where large improvements can be obtained by jet performance optimization (Pallares et al., 2005; Yin et al., 2004). Experimental analysis of these systems is made difficult by the complex chemico-physical processes controlling transport and reaction of species injected with the jet. Computational analysis offers as a cost-effective alternative to improve design and/or aid the characterization of new devices, with two main advantages: (i) performances can be tested under controlled conditions from

the early stages of design onward, and (ii) the effect of many parameters can be considered at a reduced cost with respect to the traditional experimental tests.

In this work, we present the numerical methodology developed and adopted to evaluate precisely performances of a “new concept” powder-injection system designed for the steel-making industry. The new Hi-Jet powder injector (More s.r.l.[®]) is designed: (i) to work as a burner in the early stages of the melting process and (ii) to inject carbon particles to control the chemical (and fluid dynamic) properties of the slag in the later stages. In the traditional design practice, these two tasks are performed separately by a burner and a high velocity lance: the burner feeds oxygen and methane to sustain combustion and produce heat; the lance uses a high velocity air jet to drive carbon particles toward the slag. In this configuration, due to the radial spreading of the air jet, carbon particles disperse into the

* Corresponding author. Tel.: +432 558822; fax: +432 558818.

E-mail address: marina.campolo@uniud.it (M. Campolo).

Table 1
Field test results: performances with traditional injector and with Hi-Jet injector

	Traditional injector	New-concept Hi-Jet injector
<i>Operating results</i>		
Electric energy (kWh/m ton l.s.)	365	352
Power on time (min)	31	31
Electrode consumption (kg/m ton l.s.)	1.1	1.1
Total oxygen (Nm ³ /m ton l.s.)	43.	43.3
Total natural gas (Nm ³ /m ton l.s.)	5.5	6.1
Total carbon (kg/m ton l.s.)	28.4	26.3
Charge lime + Dolo (kg/m ton l.s.)	27.	23.3
Tap temperature (°C)	1640	1650
<i>Quality/metallurgical results</i>		
Production yield (tons produced/tons charged)	92%	94%
Tapping carbon	0.035%	0.035%
Tapping oxygen (ppm)	750	750
Fe content in slag (%)	28%	22%
Metallic charge composition	86% scrap, 14% pig iron	96% scrap, 4% pig iron

m ton l.s. = millions of tons of casted liquid steel.

high temperature furnace environment, where they can burn or volatilize, thus decreasing the injection efficiency. In the “new-concept” injector, the oxygen jet issued by the burner is redesigned to promote also injection of carbon particles. This is obtained by the coaxial arrangement of streams. During injection, the inner air jet carrying the carbon particles is surrounded by an annular coaxial high velocity oxygen jet. An outer coaxial flux of methane can also be used to improve injection yield (shrouding effect). Annular nozzle sections are designed to obtain sonic flow for methane and supersonic flow for oxygen. The coaxial arrangement of streams has proven to be useful to control mixing of species in a number of industrial applications. Many experiments (see Villiermaux and Rehab, 2000; Balarac and Si-Ameur, 2005, among others) have shown that, when the outer high velocity (yet subsonic) jet is dominating, the fluid issuing from the central jet remains confined. A similar effect is expected here. Specifically, the effect of the supersonic oxygen jet on carbon particle injection is twofold: (i) it accelerates the particle laden air stream up to very large velocities; (ii) it reduces particle radial dispersion, confining and focusing particles during their flight toward the slag. These two effects are expected to increase carbon particle injection yield. Yet, for particles entrained by the oxygen-rich driving jet, the probability of burning and devolatilization may increase significantly, reducing in turn the injection yield. Therefore, an *a priori* evaluation of the injection yield which can be potentially achieved by the new injector is necessary.

Experimental evaluation of carbon particle injection yield on real operating furnaces is extremely costly and usually gives only a macroscopic indication of injection efficiency (i.e., carbon powder consumption over a given time period). Table 1 summarizes typical experimental data collected by field tests performed in a steel-making facility in Belgium (Dufenco La Luvriere S.A.). Results refer to improvements in production performance (referred to million tons of casted steel) obtained switching from a traditional injection system to the new Hi-Jet system. Among the quantities which can be used to get indirect measurements of improvement in injection performances,

the following have been considered: (i) production yield, i.e., percent of casted steel over scrap charged; (ii) ferrum content in slag, i.e., percent of metal lost as oxide in slag and (iii) metallic charge composition, i.e., relative amount of scrap and pig iron used as input. Pig iron is characterized by a high carbon content, is more expensive, and can be reduced in the charge only if carbon is efficiently fed by the injector. Field test indicates modification of the charge composition, together with an increase in production yield and a reduction in ferrum content of the slag. These information are useful to indicate process improvements, and yet insufficient to develop strategies for optimization of the injection system. In this work, we evaluate the injection yield of the new device by performing full three-dimensional numerical experiments to simulate typical operating conditions in a furnace. We consider: (i) different chemical properties and particle size distributions for injected carbon and (ii) different arrangements of the injector into the furnace (different distances from the slag) with the final aim of identifying a most critical configuration for the injector and obtaining a conservative estimate of the carbon particle injection yield.

The numerical problem is intrinsically complex because of multiphase flow, supersonic/sonic/subsonic flow transition, chemical reactions and many concurring heat transfer mechanisms. Furthermore, the chemistry of carbon particles must be described precisely to obtain reliable estimates of injection yields. At present, there is no methodology available from the shelf able to describe all these concurrent phenomena at a reasonable cost. The specific strategy adopted here to set up the numerical experiments is based on the precise fluid dynamic characterization of the reacting environment and on a chemically oriented approach which allows to use comprehensive detailed kinetic schemes for carbon particles reaction (Falcitelli et al., 2002). The methodology works as follows: first, we use state of the art numerical techniques to characterize the flow field generated by the coaxial supersonic jet issuing in the furnace. We consider the transport of the main chemical species and the minimum set of chemical reactions necessary to get

a picture of the chemico-thermal environment contributing to carbon particle oxidation and devolatilization. Second, we use Lagrangian tracking to derive detailed information about the environment seen by particles travelling inside the furnace. Third, we use these detailed information to build a simplified fluid dynamic model of the reacting environment in which more complex chemistry models for the gas phase and carbon particles are implemented (reactor network analysis (RNA)). The coupling of basic combustion modeling by the flow solver and ideal chemical reactor networks (RNA) has already been reported in previous literature (Niksa and Liu, 2002, among others). The present work represents a further contribution in this field, demonstrating that CFD + RNA modeling methodology is mature for process studies of industrial, multiphase, hot reacting systems.

The paper is organized as follows: first, we describe the different configurations investigated—including one furnace (120 ton capacity) and two positions of the injector—flow rates, carbon particle size distributions and chemical properties of carbon—; second, we discuss the numerical methodology, including the domain discretization, the modelling assumptions and numerical algorithms; third, we present the results, focusing on carbon particle injection yields, i.e., fraction of injected carbon reaching the slag (i.e., not volatilized and burnt during the flight toward the slag) and we evaluate the effect of injector position, carbon particle size distribution and chemical properties; finally, we summarize the conclusions of our analysis.

2. Problem and data

2.1. Reference configuration

The reference geometry analysed in this work is shown in Fig. 1, together with a close-up of the injection device.

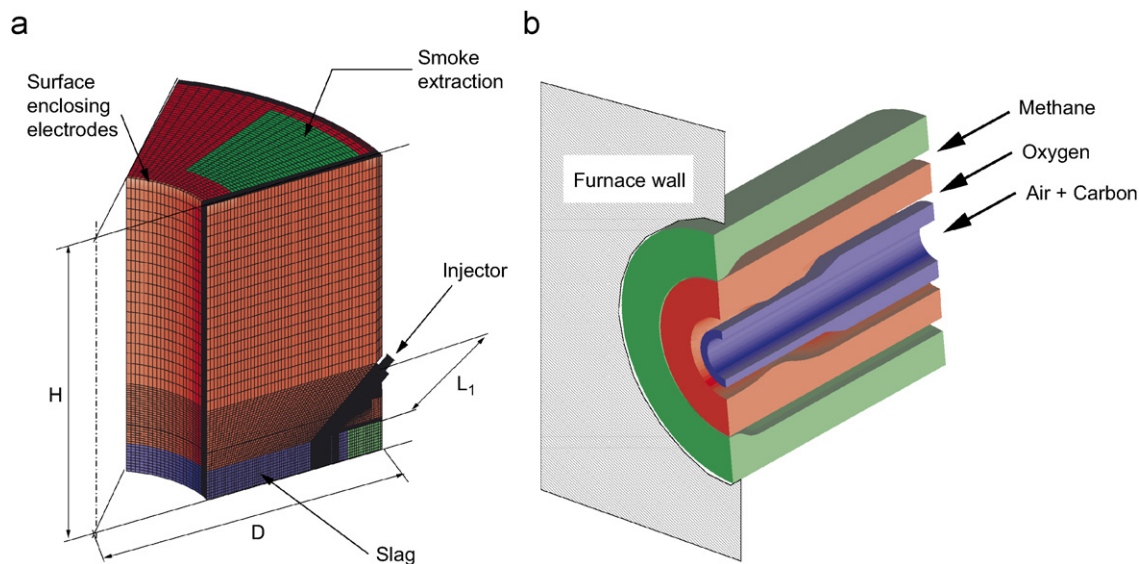


Fig. 1. (a) Dimensions and discretization of the computation domain for the numerical simulation; (b) detail of the injection system: particle laden air jet is issued from blue pipe, supersonic oxygen jet is issued from red pipe and sonic flow of methane is issued from green pipe.

The injector is installed in a 120 ton capacity electric arc furnace (EAF). Furnace diameter and height are 6.9 and 3.640 m, respectively, and the furnace is equipped with three electrodes (102 MW power) and four injectors.

Two different distances of the injector from the slag ($L_1 = 977$ mm and $L_2 = 1377$ mm) are considered and reference working conditions as summarized in Table 2. Injection efficiency is evaluated considering two different size distributions and different types of carbon, summarized in Table 3.

We consider also two external factors influencing carbon particle injection efficiency, i.e.: (i) air uptake from the top cover of the electric furnace and (ii) radiation effects from furnace walls, electrodes and slag (see Table 4). For point (i), we place the carbon injector below the air uptake (fourth hole) to simulate the worst condition for jet deformation, in which smoke extraction from the furnace may entrain and separate particulate carbon from the jet stream. As shown in Fig. 1, we model the fourth hole as a rectangular section (in green), equivalent in area to the circular section found in real installations. We verified that this simplification has no consequences on the deformation of the jet due to the smoke extraction system. For point (ii), we simulate explicitly carbon particles moving toward the slag which may burn or volatilize when exposed to high temperatures, considering also radiation effect and heat transfer inside the EAF.

2.2. Geometry and computational domain

Fig. 1(a) shows the portion of the furnace considered to perform the numerical simulations. Fig. 1(b) shows a close-up of the supersonic injector which is composed by three different ducts. The outer (green) duct feeds the methane; the intermediate (red) duct feeds the oxygen and the inner (blue) duct feeds the air flow laden by carbon particles.

The furnace is equipped with four of these injectors. Due to the complexity of the furnace geometry, we simulate only 45°

Table 2
Mass flow rates and stagnation conditions for the streams feeding the injector

	Mass flow rate (Nm ³ /h)	Stagn. temp. (K)	Stagn. press. (bar)
Methane	80	288.8	1.046
Oxygen	2900	289.02	12.9
Air	80	288	–
Carbon particles	27 kg/min		–

Mass flow for carbon particles.

Table 3
Particle size distributions and properties of carbon particles

	Size distribution	
	Rosin–Rammler A	Rosin–Rammler B
D_{\min}	0.106 mm	0.1 mm
D_{\max}	2. mm	3. mm
D_{ave}	0.295 mm	1.85 mm
n	2.378075	3.356697
Shape factor	0.7	0.7
	Carbon properties	
	Petrolcoke	Anthracite
ρ_C	1400 kg/m ³	1400 kg/m ³
H_{inf}	8176 kcal/kg	7600 kcal/kg
H_{sup}	8365 kcal/kg	8500 kcal/kg
$m_v/m\%$	13.07	7.5
Fixed carbon	86.61	87.7

Table 4
Data used to model the effect of external factors affecting particle injection efficiency

Boundary conditions		
Air uptake	Flow rate	65,000 (Nm ³ /h)
Radiative effects	Wall temperature	1673.15 K
	Top temperature	1673.15 K
	Slag temperature	1923.15 K
	Wall and slag emissivity	0.7
	Electrode emissivity	0.8
	Electrode temperature	980–2380 K

of the furnace, i.e., the minimal periodical portion extending from the injector symmetry plane to the plane in between two injectors. The liquid steel and electrodes are not included in the computational domain.

The domain is bounded: (i) by the slag (blue region) at the lower side; (ii) by the top wall and by the exhaust extraction section (in green) at the upper side and (iii) by a section enclosing the electrodes at the inner radial side.

The computational domain shown in Fig. 1 is made of about 340,000 cells. The mesh is finer near the injector to simulate precisely the gradients of velocity, temperature and mass fraction profiles which are largest in this region.

Additional boundary conditions used to set up the numerical simulation are: (i) symmetry plane at the jet middle plane; (ii) no-slip boundary condition for gas velocity at solid walls; (iii) fixed pressure (1 atm) on the side surface; (iv) fixed temperature profile and emissivity values for radiative heat transfer at the walls, at the surface enclosing the electrodes and at the bottom surface (Guo and Irons, 2003); (v) fixed mass flow rate for oxygen, methane and air at the injection point; (vi) fixed outgoing mass flow rate (65,000 Nm³/h) at the smoke exit.

3. Methodology

The problem under study is characterized by: (i) multiple streams of different gases (air, methane, oxygen) fed into an atmospheric air environment; (ii) supersonic/sonic conditions for some of the streams; (iii) chemical reaction between oxygen and methane; (iv) heat transfer/production affecting fluid dynamic behaviour of the flow; (v) multiphase flow and complex kinetics for carbon particles injected and moving in a reactive environment (high temperatures and large oxygen mass fraction). Since there is no methodology available from the shelf able to describe all these concurrent phenomena precisely and at a reasonable cost, all these points have been addressed using state of the art techniques for the modelling, based on a commercial finite volume solver of Navier–Stokes equations (Star-CD[®]) coupled to *ad hoc* research tools (Lagrangian tracking routines and detailed kinetic models for carbon particles). The methodology is discussed briefly in the following sections.

3.1. Flow field, thermal field and scalar field calculation

The flow generated by a coaxial arrangement of streams has been extensively studied in the literature, both in the case of incompressible fluid (see Rehab et al., 1997; Balarac and Metais, 2005, among others) and in the case of compressible fluid (Dahal and Morris, 1997). The flow is controlled by the growth rate of the shear mixing layer at the interface between the inner and the outer jet. Very accurate experiments or numerical analyses are required to capture the time dependent nature of this flow (see, for instance Pantano and Sarkar, 2002; Freund et al., 2000). Yet, these approaches cannot be used here, where the supersonic jet is simulated inside a complex environment corresponding to the electric arc furnace. A simplified numerical approach based on a commercial finite volume solver of RANS equation has been used. The flow is compressible and simulated as an ideal mixture of gases. Equations governing mass, momentum and heat transfer in the EAF are Navier–Stokes equations and chemico-thermal enthalpy balance. Equations are solved for a carrier fluid (air) and turbulence effects are accounted for using a $k-\epsilon$ turbulence model (Patankar and Spalding, 1972). In coaxial supersonic flows, the turbulence field is affected by the velocity ratio of streams, by the relative difference in velocity and by compressibility effects (density ratio of streams) which may contribute in suppressing turbulence at the interface between streams

(Urban and Mungal, 2001). This effect has been accounted for using a modified $k-\epsilon$ model in which a correction for compressibility is added (see Sarkar et al., 1991). Equations are used together with ideal gas law to link pressure and density to local temperature of the compressible fluid.

In this work, the flow field produced by the cold supersonic jet of oxygen is modified by the chemical reactions of oxygen with: (i) methane issued by the outer coaxial jet and (ii) carbon mono-oxide already present in the furnace or produced from methane combustion. Mixing between reactants controls the rate of reaction and heat production in the region of the supersonic reacting jet. Heat released by these two reactions may contribute to gas density reduction producing further acceleration of the jet. Furthermore, the jet region is coupled with the outer computational domain through radiative effects, both from the flame to the surrounding and from the radiative surfaces (side wall, slag, electrodes) back to the flame. It is really complex to make the problem numerically tractable by a CFD code, retaining all the relevant phenomena. In this work, we decided to simplify the chemistry considering a reduced reaction scheme for methane oxidation which is written as:



Conservation of mass is solved for each relevant chemical species. Reaction rates are calculated using the Eddy Break up model (Magnussen and Hjertager, 1981), considering that the rate-controlling mechanism may be either the chemical kinetics or the turbulent mixing. In this way, we try to take into account the effect that local micro-mixing may have in the determination of the rate of reaction (Marchisio and Barresi, 2003). The two steps approximation used to model the combustion process is rather crude and does not allow to simulate precisely important characteristics of methane oxidation, as mass fraction of secondary species and flame temperature. Specifically, the adiabatic flame temperature is over-predicted when dissociation of chemical species is significant and is not accounted for. Thermodynamic calculations indicates that the adiabatic flame temperature calculated for the methane/oxygen reactions when dissociation of species is taken into account is $T_{\text{ad}} = 3053$ K (Baukal, 1998). The dissociation of CO_2 and O_2 (both of which are strong endothermic reactions) is indeed significant (Li and Fruehan, 2003) at this temperature (molar concentration at equilibrium is 15.5% CO , 11.3% CO_2 , 4.8% H , 7% H_2 , 40% H_2O , 3.8 % O , 9.9% OH and 8.1% O_2 from Baukal, 1998). Temperature values calculated by our numerical simulation under operative conditions (i.e., radiative effects to and from walls of the furnace), should not be larger than the adiabatic value, T_{ad} . In this work, we are not concerned with the detailed chemistry of the methane and carbon mono-oxide combustion processes, whereas we need to simulate precisely the gas temperature to account for variations in gas density and velocity which control the transport of carbon particles. Therefore, we decided to bound the temperature increase due to the heat of reaction reducing numerically the reaction rate when the temperature rises

up to T_{ad} , keeping the number of simulated species as low as possible. From the fluid dynamic point of view, this allows to reproduce a realistic thermal field, containing the costs of the simulation.

3.2. Lagrangian particle tracking

For injection conditions examined in this work, it is difficult to evaluate a priori whether the gas particle flow is concentrated or diluted. From data shown in Table 2, the mass loading is about 16 in the pipe feeding carbon particles and decreases to 0.42 if we consider carbon particles entrained in the supersonic jet flow. Volume fractions are 1.4% in the feeding pipe and 0.0384% in the jet, indicating a particle interspace distance from 3 to 10 times the particle diameter. Therefore, real conditions correspond to a dense flow in the feeding pipe which becomes diluted as soon as particles enters the EAF and are accelerated by the supersonic jet. Since we are concerned with particle transport inside the EAF, we assume that particles entering the furnace are dilute enough to consider particle/particle interaction negligible and to neglect particles feed back on the fluid (one-way coupling). Motion of carbon particles in the carrier fluid is simulated by solving the momentum equation for each single particle, given by

$$m_p \frac{dv_p}{dt} = F_D + F_G + F_B + F_L + F_{Bs} + F_{PG} + F_{VM}, \quad (3)$$

where, m_p is particle mass, v_p is particle velocity and terms on the RHS represent drag, gravity, buoyancy, lift, Basset, pressure gradient and virtual mass forces. In particle-laden flows, the key parameter controlling dispersion is the Stokes number (St), i.e., the ratio between the particle aerodynamic response-time and the relevant flow time scale. In this work, the relevant flow time scale is given by the supersonic injector diameter divided by the supersonic jet velocity (about 10^{-4} s). According to many previous works (see, for instance, Chung and Trout, 1988; Loth, 2000; Campolo et al., 2005), the study of the order of magnitude of the forces acting on particles based on the equation of motion derived by Maxey and Riley (1983) reveals that, compared to the inertial term which is $O(1)$, the drag force is $O(St^{-1})$, the virtual mass and the pressure gradient are $O((\rho/\rho_p)^1)$ and the Basset force is $O((\rho/\rho_p)^{1/2})$, where ρ and ρ_p are fluid density and particle density, respectively. In our work, $\rho/\rho_p \simeq O(10^{-3})$ and St based on the reference time scale for the fluid, is in the range $[10^0/10^2]$. Therefore, for the specific flow system examined here, virtual mass is negligible ($O(10^{-3})$), drag is significant ($O(10^{-2}-1)$), Basset force is negligible ($O(10^{-2})$) at least for the smaller particles. From a conservative estimate of the time of flight ($t_{\text{travel}} \simeq L/U_{\text{air}} = 8.5 \times 10^{-3}$ s), we decided to neglect gravity since the contribution of gravitational acceleration to particle vertical motion is negligible (less than 0.1%) with respect to the vertical motion produced by the starting component of downward velocity. Therefore, for a carbon particle in a gaseous stream all the forces on the RHS except the drag force may be neglected. Under these assumptions, the equation of particle motion may

be written as

$$\frac{dv_p}{dt} = \frac{3}{4} \frac{C_D}{D_p} \frac{\rho}{\rho_p} \|v - v_p\| (v - v_p), \quad (4)$$

where t is time, v_p , D_p and ρ_p are particle velocity, diameter and density, respectively, v and ρ are fluid velocity and density and the drag coefficient, C_D , is a function of the particle Reynolds number, $Re_p = \rho D_p \|v - v_p\| / \mu$, which depends on the (instantaneous) relative difference between particle velocity and fluid velocity at the particle position.

In this work, the calculation of the drag coefficient should take into account two different effects: (i) particles move into a supersonic flow; (ii) carbon particles are not spherical (shape factor 0.7). We should remark here that both these effects contribute by increasing the drag coefficient. Compressibility effects can be evaluated using the correlations derived by Carlson and Høglund (1964). Shape factor effects can be evaluated using the correlations derived by Haider and Levenspiel (1989) and discussed in Crowe et al. (1998). Corrections are of the same order and there is no reference in the literature on the way they should be combined together. Therefore, to be conservative in our simulations, we decided to account for shape factor modifications only and the drag coefficient is calculated as $C_D^{ms} = C_D \cdot K_f(\psi, Re_p)$ where K_f is the effective drag factor. In this work, we consider a particle shape factor equal to 0.7 and K_f is taken from Crowe et al. (1998).

Particle equation is discretized using finite-differences and integrated explicitly in time using a time step which is 1/20 of the smallest particle characteristic time, $\tau_p = \rho_p D_p^2 / 18\mu$. Tri-linear interpolation of fluid velocity values available at grid points is used for the calculation of drag force which requires evaluation of fluid velocity at particle position. Since the flow is turbulent, the instantaneous fluid velocity at particle position is obtained from the calculated flow field and from the local turbulence field (turbulent kinetic energy and turbulent dissipation) using the eddy interaction model by Gosman and Ioannides (1983) and Graham (1998).

The size distribution of carbon particles injected into the furnace determines their behaviour in the external flow. Table 3 summarizes distributions analysed in this work. Specifically, we track many classes of particles with diameter in the range $[D_{\min} - D_{\max}]$. For each class of particles, we use trajectory data to calculate the radial dispersion and the time of flight distribution. Statistics for the swarm are reconstructed from results obtained for each class of particles weighted by the corresponding mass particle size distribution (see Table 3).

3.3. Reactor network analysis

For modelling purposes, carbon particles are described in terms of a solid fraction, a volatile fraction and an ash forming fraction. For carbon particles injected by the jet and moving toward the slag, solid and volatile fractions are reduced by: (i) char combustion and (ii) devolatilization, which contribute in parallel to mass consumption. The chemical environment seen by carbon particles plays a significant role for the determination of reaction rates. It can be reproduced precisely using

complex gas phase reaction mechanisms (i.e., a core hydrocarbon combustion model, as developed by Ranzi et al., 2001, nitrogen sub-mechanisms, as developed by Coelho et al., 2001 and additional mechanisms if required by the specific application). Then, char combustion can be evaluated solving the mass and thermal balance written for the particles and devolatilization can be modelled as a single first order reaction (SFOR) considering the detailed thermal history of particles. Introducing such complex kinetics in detailed three-dimensional numerical simulations is not cost-effective, since hundreds of chemical species or radicals and thousands of chemical reaction should be considered for the gaseous phase. An alternative, effective approach successfully used in the literature is RNA: based on the results of numerical simulations, the fluid dynamic domain is simplified by an automatic zoning algorithm as an equivalent network of ideal, perfectly stirred, reactors. Detailed homogeneous and heterogeneous reaction mechanisms are then applied over the reactor network to perform accurate calculation of gas phase reactions, char combustion and carbon devolatilization to evaluate precisely injection yield (Falcitelli et al., 2002).

In the case under study, we use statistics derived from Lagrangian tracking to characterize the environment seen by carbon particles and to identify the equivalent series of perfectly stirred reactors, as shown in Fig. 2. Characteristics of each reactor (i.e., volume, residence time, temperature and mass fraction of main species) are determined from the conditions calculated locally by the flow solver. Within each reactor of the network, homogeneous gas chemistry is coupled with the heterogeneous chemistry describing carbon particle oxidation through a fundamental formulation of the mass balance (see Pedersen et al., 1998).

Char oxidation is controlled by diffusion of oxygen toward the surface of the carbon particle. Char oxidation rate is described by a semi-empirical expression given by a 0.5 order kinetic rate

$$N_C = k_s (P y_s)^{1/2}, \quad (5)$$

where N_C is char oxidation rate, ($\text{kg C/m}^2 \text{ s}$), k_s is the kinetic constant, ($\text{kg C/m}^2 \text{ s Pa}^{0.5}$), P is the total pressure and y_s is the oxygen mass fraction at the surface of the particle, combined with a diffusion resistance

$$N_C = h_g \ln \left(\frac{v/(1-v) + y_b}{v/(1-v) + y_s} \right), \quad h_g = D \frac{\rho_p}{R_p} \left(\frac{1}{1-v} \right), \quad (6)$$

where y_b is the oxygen mass fraction in the bulk, D is the oxygen diffusion coefficient, R_p is the particle radius and v is the number of moles of O_2 reacted per mole produced by the oxidation.

The kinetic constant, k_s , is given by

$$k_s = A \exp \left(- \frac{E_a}{RT_s} \right), \quad (7)$$

where A and E_a depends on char composition and are estimated using correlations based on experimental data taken from Hurt and Mitchell (1992) and T_s is the temperature at particle surface. Eqs. (5) and (6) are coupled through T_s with the

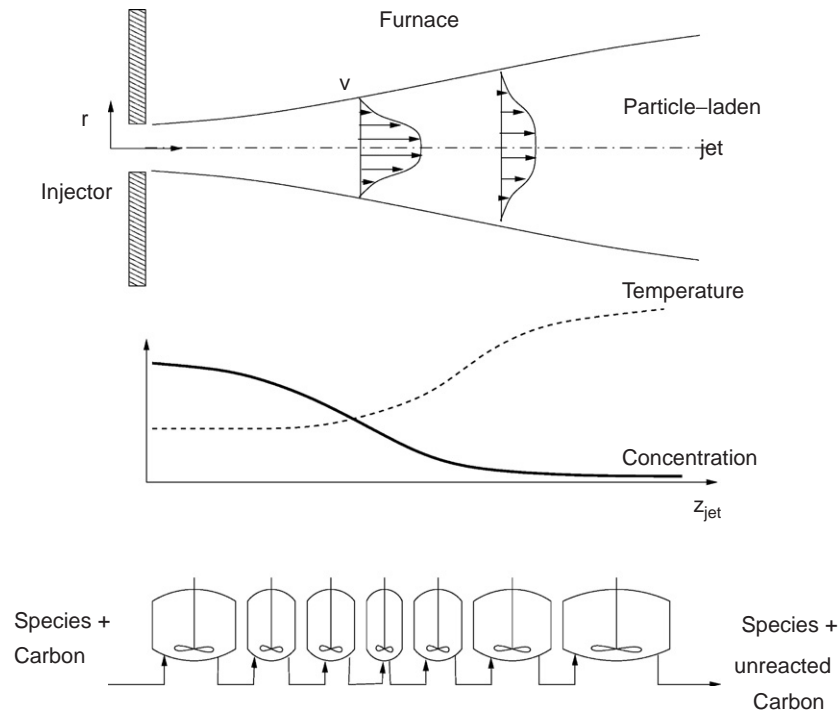


Fig. 2. Reactor network analysis (RNA) simplification of real environment.

particle thermal balance equation in which the contribution of convection, radiation and heat produced by the chemical reaction is accounted for. Eqs. (5) and (6) and thermal balance are jointly solved by iterations to obtain the instantaneous value of the surface temperature of the particle, T_s , the rate of reaction, N_C , and the oxygen mass fraction at the surface of the particle, y_s . Reaction rates are calculated for different size particles and particle size distribution is updated over time as particles move from one reactor to the other.

Devolatilization is assumed to take place in parallel with char oxidation. This is a conservative assumption for carbon consumption since in real conditions the volatile flux coming out from the particle may prevent oxygen diffusion toward the particle surface, reducing the oxidation. Two different approaches have been considered to evaluate the effect of devolatilization. In the first approach, following Badzioch and Hawksley (1970), devolatilization is modelled as a SFOR process, with a reaction rate proportional to the amount of volatile matter still remaining in the coal:

$$\frac{dV}{dt} = k_v(V^* - V), \quad (8)$$

where V is volatile mass released at time t and V^* is the initial volatile content. The rate constant, k_v , is correlated with temperature by an Arrhenius expression

$$k_v = A_v \exp\left(-\frac{E_v}{RT_p}\right) \quad (9)$$

with A_v and E_v pre-exponential factor and activation energy. In the second approach, a number of different volatile constituents of coal are considered, for each of which devolatilization is

modelled as a first-order reaction process. Constituents are characterized by a slightly different reaction rate, due to variation of the activation energy, described by a Gaussian distribution (DAEM, distributed activation energy model). This model gives a better representation of coal devolatilization since it captures the different time scales of the process (Please et al., 2003). The overall mass of volatile matter is calculated by integration of the volatile mass released by the different constituents, which can be written in a simplified form as

$$\frac{dV}{dt} = \langle k \rangle (V^* - V), \quad (10)$$

where $\langle k \rangle$ is a time dependent rate constant. With respect to Pedersen et al. (1998), some novel characteristics of the solver for heterogeneous chemistry are: (i) a huge number of size/burnout classes for char particles; (ii) the characterization of each char particle by its ash forming matter; (iii) the use of an integral (rather than differential) population balance; (iv) the possibility of specifying a slip between gaseous and solid time contact for each size/burnout class, and (v) the solution of the system of equations at the same time in both gaseous and solid phases. We refer to Falcitelli et al. (2002) for a more detailed description of the simulation of the two-phase combustion model.

4. Results

Simulations have been performed for two different positions of the injector in the furnace. Results are discussed into detail for one configuration (L2) since “a posteriori” analyses have

shown that this is the most critical configuration to evaluate carbon particle injection yields.

Flow field, species mass fraction and temperature field are presented to characterize the furnace environment calculated numerically. The flow field determines (i) transport and mixing of chemical species issued by the injector and (ii) transport and dispersion of carbon particles. In turn, residence time and chemico-thermal environment seen by carbon particles control their rate of reaction and devolatilization in the EAF.

4.1. Flow field characterization

Fig. 3(a) shows velocity iso-contours in the jet symmetry plane for injector position *L2*. Values range from a maximum of 520 m/s for the supersonic oxygen stream to zero for the outer flow. The high velocity region generated by the annular oxygen stream spreads radially as the jet moves into the furnace. The jet axial velocity reduces progressively as the jet penetrates into the furnace. When the jet impinges against the slag, expanding parallel to the slag surface, a high velocity core of the jet (about 320 m/s velocity) is still present. The same trend is observed for position *L1* (not shown here).

The high velocity oxygen jet accelerates strongly the inner, slower air jet used to inject carbon particles. Fig. 3(b) shows the variation of jet velocity along the axial coordinate. Negative coordinates correspond to positions inside the feeding pipe. Blue and red lines correspond to injector position *L1* and *L2*, respectively. For both injector positions, the velocity drops down at the jet exit where a recirculating zone exists (see the pale blue zone downstream the nozzle exit in Fig. 3). Further downstream, air is strongly accelerated by the high velocity oxygen jet up to 433 m/s for injector position *L1* and up to 430 m/s for injector position *L2* (Mach number about 1.3). The maximum velocity, which is obtained 870 mm (*L1*) and 850 mm (*L2*) downstream the nozzle, decreases as the jet approaches the slag (977 and 1377 mm, respectively). Velocities in other parts of the EAF are about 5–10 m/s, with larger values in the regions where the jet entrains outer fluid and where the fourth hole is extracting air.

4.2. Mass fraction of species

The local flow field at the jet exit controls the transport of injected species which, in turn, determines the progress of methane/oxygen combustion. Fig. 4 shows the mass fraction of oxygen, carbon oxide, carbon dioxide and water in the jet symmetry plane for injector position *L2*. The high velocity oxygen stream entrains methane (not shown) which mixes rapidly with oxygen. Due to combustion and excess of oxygen, the mass fraction of methane becomes almost negligible right downstream the nozzle, where all the fuel is burnt. High mass fraction of oxygen is found all along the jet trajectory up to the slag. Mass fraction decreases from 1.0 (at the nozzle exit) to 0.65 when the jet reaches the slag.

Fig. 4 shows also the mass fraction of CO. Mass fraction in the outer flow is fixed at 0.4 to represent the atmosphere of the

EAF environment, is zero in the central region of the jet, filled by oxygen and gradually increases across the jet boundary. Reaction between oxygen and CO occurs at the outer surface of the jet, encapsulating the flow of air into an high temperature envelope which promotes the acceleration of carbon particles toward the slag (Li and Fruehan, 2003).

The mass fraction of water identifies the regions in the computational domain where the reaction between oxygen and methane occurs, corresponding to the annular envelope found at the outer boundary of the oxygen jet. A small quantity of water forms also in the lower part of the jet. Similarly, the mass fraction of CO₂ can be used to identify the regions where the second step of the chemical reaction occurs. CO₂ forms in the whole region surrounding the oxygen jet. High mass fraction of CO₂ is found especially in the region below the jet, where the flow field is characterized by low velocity values and recirculation of fluid is observed in the region confined by the jet, the wall of the furnace and the slag surface.

4.3. Temperature field

Fig. 5 shows the effect of combustion on the temperature field. Environmental temperature in the EAF is set equal to 1500 °C (1773 K). Fig. 5(a) (injector position *L2*) shows that the largest temperature values are found in the region where methane and oxygen burn to produce water. Lower values of temperature are found in the region where CO and O₂ react to give CO₂. The lowest values of temperature are found along the jet axis, associated with unreacted oxygen. A similar behaviour is observed for injector position *L1*. Fig. 5(b) shows the thermal profile along the jet axis for both configurations. In the jet axis region, where oxygen is issued at 288 K, the temperature rise due to combustion and thermal radiation is the same for injector position *L1* and *L2* up to 800 mm from the jet exit. Further downstream, due to the radiative effect from the liquid metal at the bottom of the furnace, the temperature rises up to 400 K (*L1*) and up to 1400 K (*L2*) as the oxygen moves toward the slag.

4.4. Carbon particles

4.4.1. Swarm dispersion

For the Lagrangian analysis, we consider the poly-dispersed swarm of particles made of groups of different size particles, as prescribed by the Rosin–Rammler distribution. Each class of particles is tracked over time from the injection point to the slag. Simulating many groups of particle diameters has two main advantages: on the one hand, we can characterize the overall behaviour of the swarm; on the other hand, we can identify size-dependent effects which may influence significantly oxidation and devolatilization dynamics. Results of the Lagrangian analysis are presented both: (i) in aggregated form (with reference to the particle size distribution) and (ii) for minimum, maximum and average diameter of the particle size distribution.

Carbon particles are in equilibrium with the air jet (i.e., move at the same velocity) when they are injected into the furnace

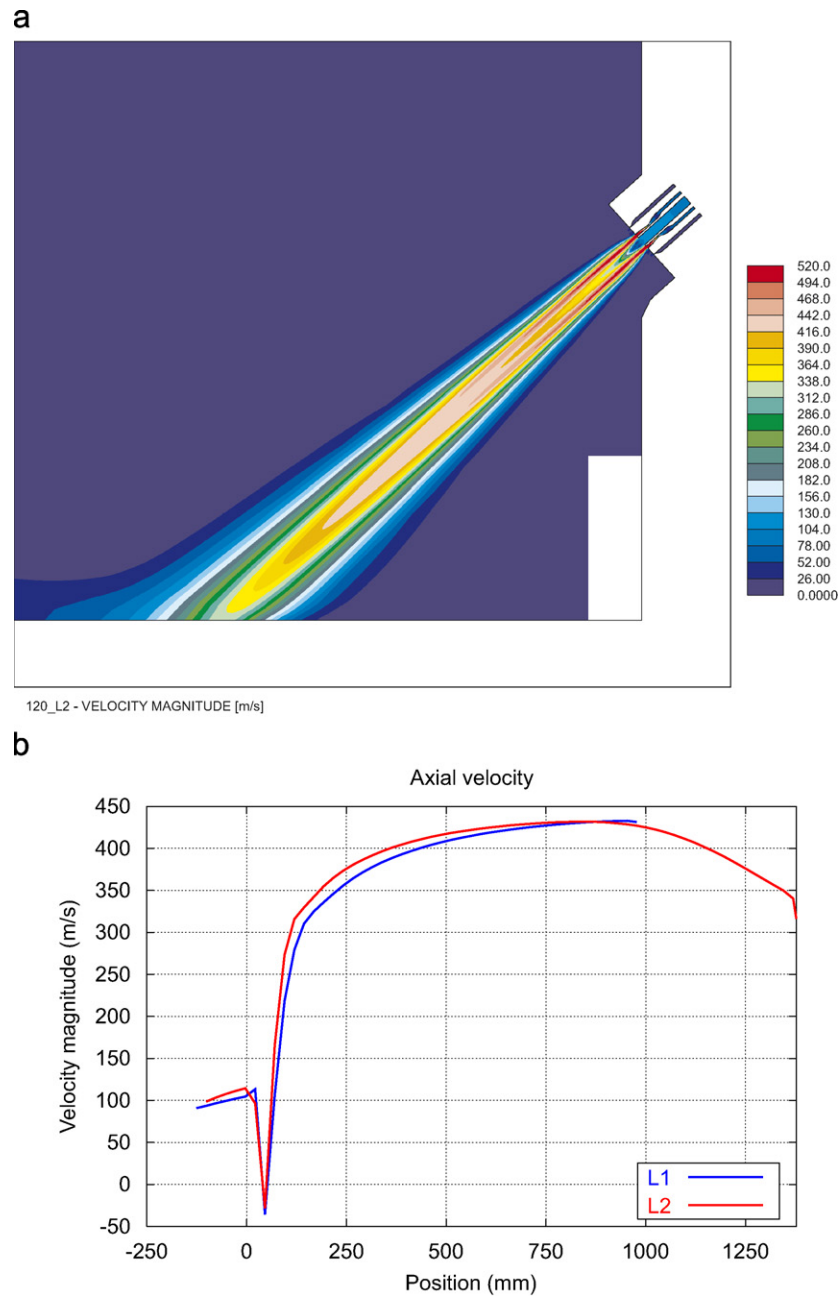


Fig. 3. (a) Velocity magnitude in the jet symmetry plane (injector position L2); (b) velocity magnitude along the jet axis for injector position L1 and L2. The slag is at 977 mm (L1) and at 1377 mm (L2), respectively.

and experience a strong acceleration as the air flow is entrained by the supersonic oxygen jet. Carbon particles response to these velocity variations strongly depends on particle inertia: due to the short path to travel, there is no time for the particles to reach a new equilibrium with the carrier fluid and particle velocity inside the coaxial jet remains everywhere smaller than the local fluid velocity.

Fig. 6(a) shows a snapshot of the swarm of particles ($D_p = 0.2 \text{ mm} = 200 \mu\text{m}$, i.e., average diameter value of RR-A distribution) superposed to fluid velocity iso-contours. Only a few particles are shown, colored according to particle velocity. We observe that $200 \mu\text{m}$ particles are accelerated from 80 m/s , i.e.,

the air velocity in the duct, to 340 m/s , which is less than the local fluid velocity.

Fig. 6(b) shows the same particles colored with the temperature of the background fluid in which they are moving, superposed to oxygen mass fraction iso-contours. Temperature and oxygen mass fraction are the main factors controlling (i) heat transfer to particles moving in the EAF and (ii) rates of oxidation and devolatilization. Since particles remain focused around the jet axis, the background fluid sampled by particles moving in the EAF is the oxygen stream issued from the nozzle, which is colder than the outer fluid in the furnace. Moreover, due to the short travel time inside the furnace,

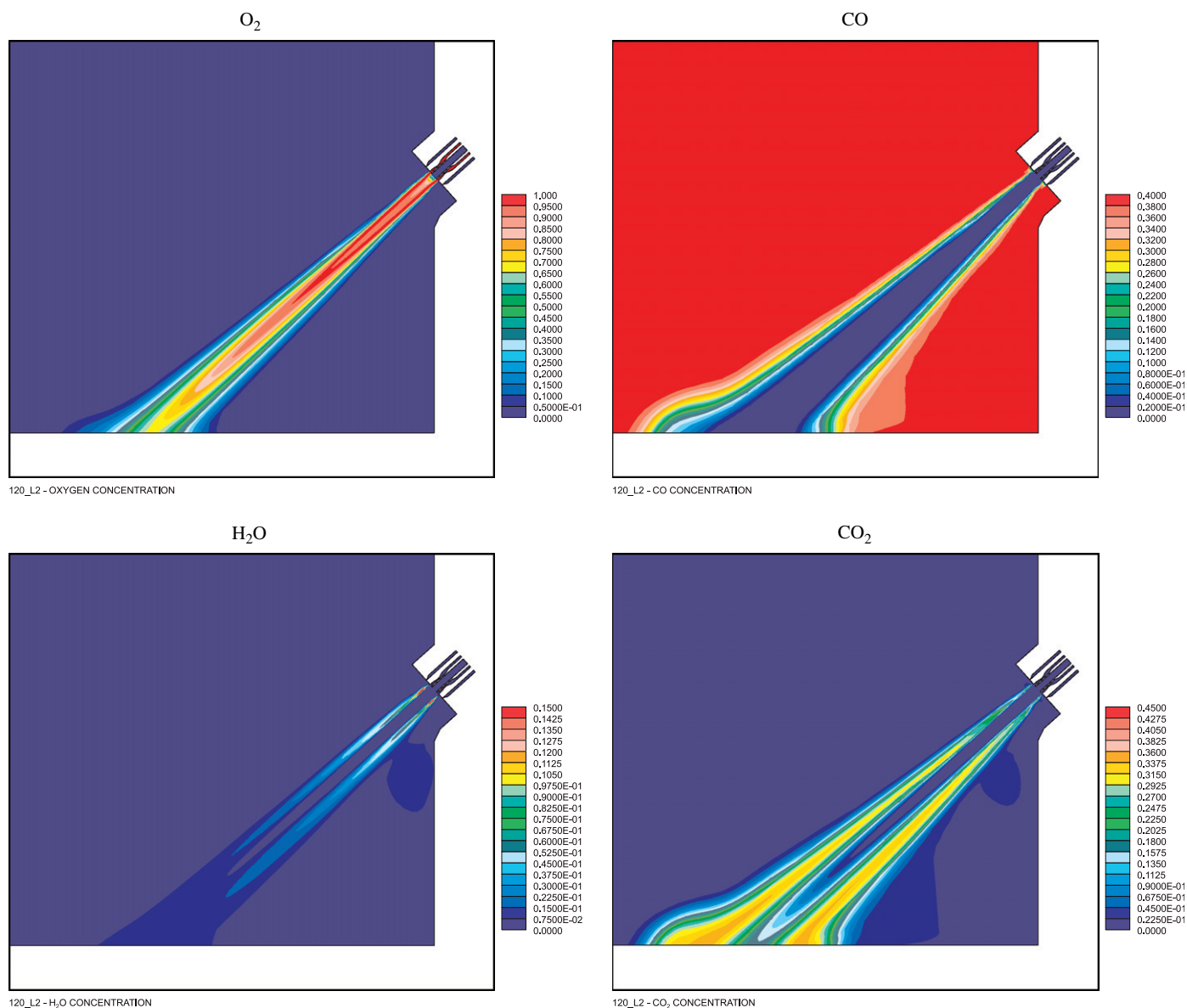


Fig. 4. Details of the mass fraction field for O₂, CO, H₂O and CO₂ at the jet symmetry plane. Injector position L2.

conductive, convective and radiative heat transfer are found to contribute negligibly to particle heating, decreasing the probability of carbon devolatilization.

Fig. 6(a) and (b) shows that information on particle radial distribution and velocity distribution are crucial to evaluate oxidation and devolatilization of carbon particles, since the radial dispersion of the jet determines temperature and oxygen mass fraction seen by particles whereas the evolution of velocity determines the residence time of particles inside the reacting environment. These effects have been considered to identify the characteristics of the net of equivalent reactors which have been used to reproduce in a simple way the EAF environment. Results from the Lagrangian tracking are discussed here in terms of: (i) radial dispersion; (ii) residence time distribution since these informations have been used to size the equivalent net of reactors.

4.4.2. Radial dispersion and velocity distribution

Particles distribution is uniform in the radial direction inside the feeding pipe (11.5 mm radius). This distribution changes as particles move with the jet, spreading radially. Fig. 7 shows the radial distribution of particles at five different distances from the point of injection (respectively 250, 500, 750, 1000 and 1250 mm, from bottom to top) and injector position L2. Data on the left and on the right refer to carbon particle size distributions RR-A and RR-B, respectively.

Comparison between results obtained for distributions RR-A and RR-B shows that RR-B particles, which are larger and therefore more inertial, remain more focused than RR-A particles. This is expected since larger particles respond less to local velocity variations and move almost decoupled from the flow, following their inertia. For both size distributions, the radial dispersion at 1250 mm, i.e., slightly upstream of the slag,

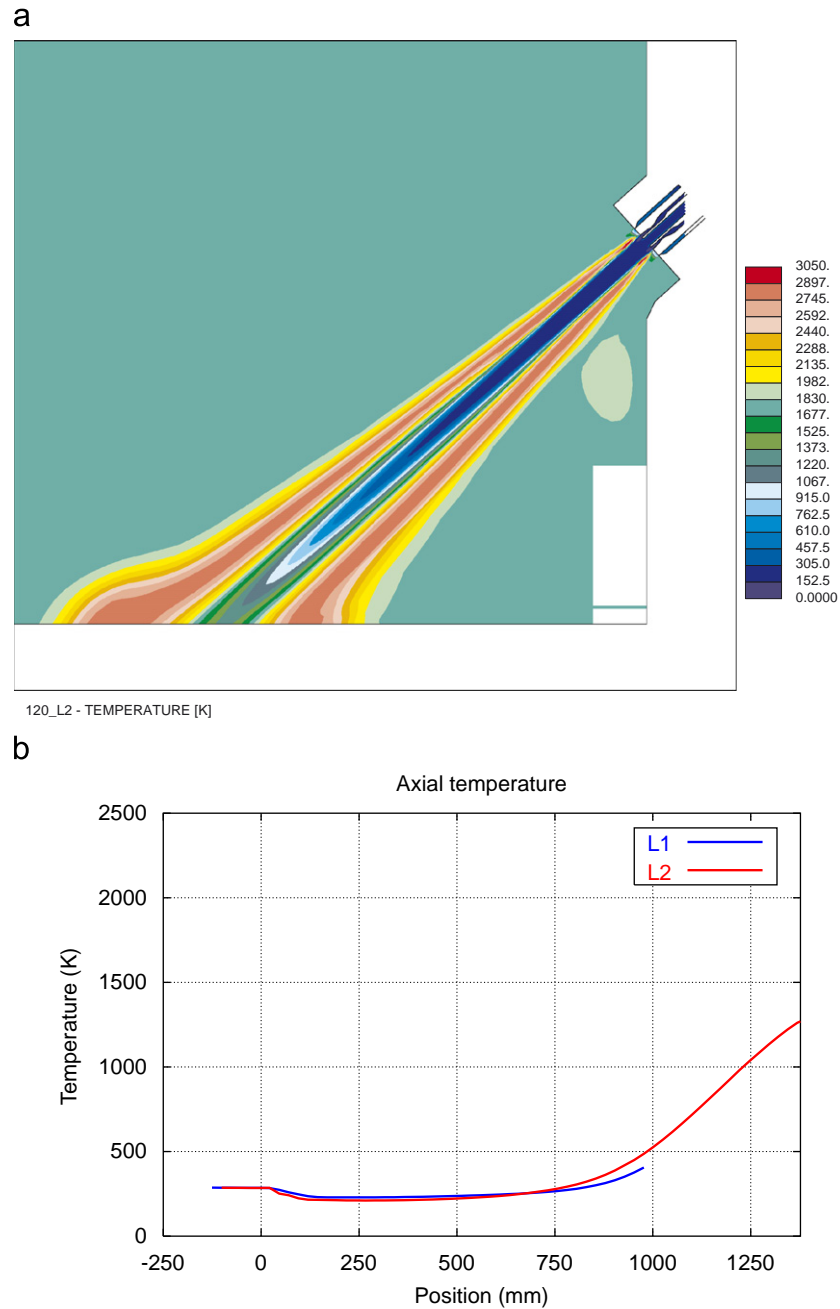


Fig. 5. (a) Temperature field at the jet symmetry plane; (b) temperature field along the jet axis for injector position L1 and L2. The slag is at 977 mm (L1) and at 1377 mm (L2), respectively.

is rather small, indicating that particles remain focused into a narrow region of the jet.

Fig. 8 shows the evolution of the velocity distribution of the same particles. At inlet, particle velocities for both distributions are set equal to the air velocity (about 80 m/s). As the particles move inside the furnace, the drag force accelerates them toward the local fluid velocity. Comparing results obtained for distributions RR-A and RR-B, we observe that RR-A particles accelerate more than RR-B particles since they have a smaller mean response-time. Nevertheless, since the response-time of both particle distributions is larger than the time spent into the

furnace, they have no time to reach a new equilibrium with the fluid, and particles move always slower than the jet fluid. Compared to injector position L1 (results not shown here), for position L2 particles gain a larger velocity before reaching the slag due to a larger time of flight.

4.4.3. Lagrangian characterization of EAF environment

Characteristics of the reactive environment seen by particles of the two Rosin Rammler distributions are summarized in Fig. 9. Specifically, the travel time, the thermal field and the oxygen mass fraction sampled by particles are considered.

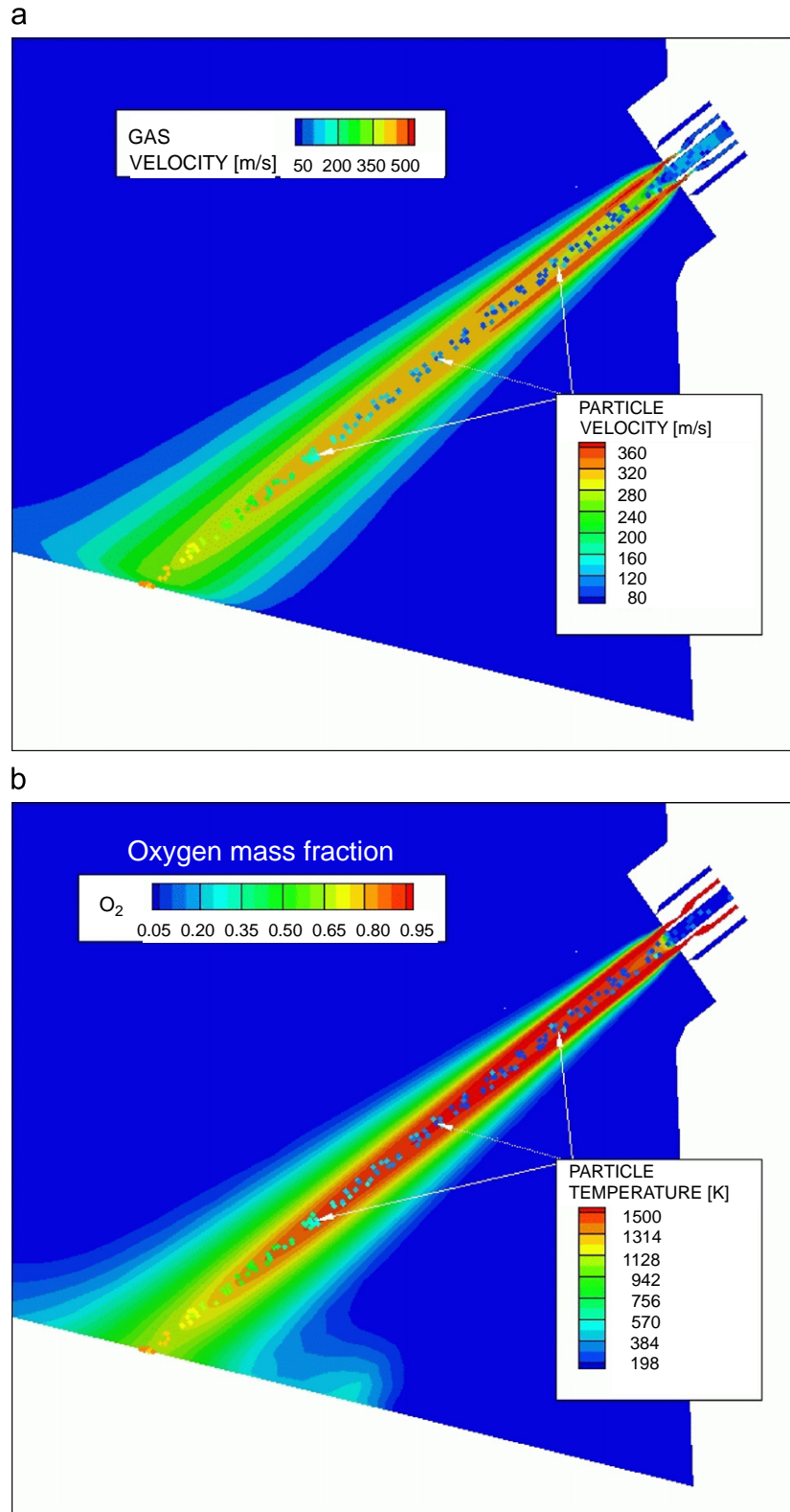


Fig. 6. (a) Velocity of carbon particles in the jet symmetry plane; (b) temperature field at particle positions in the jet symmetry plane and oxygen mass fraction iso-contours. Injector position $L2$. Particle diameter is 0.2 mm (average D_p for RR-A).

Fig. 9(a) shows the travel time distributions calculated for RR-A and RR-B particles and injector position $L2$. The average travel time for RR-A particles is smaller than for RR-B

particles and the distribution is more concentrated around the mean. Table 5 summarizes mean and variance of the travel time distributions for injector position $L1$ and $L2$. Data from the

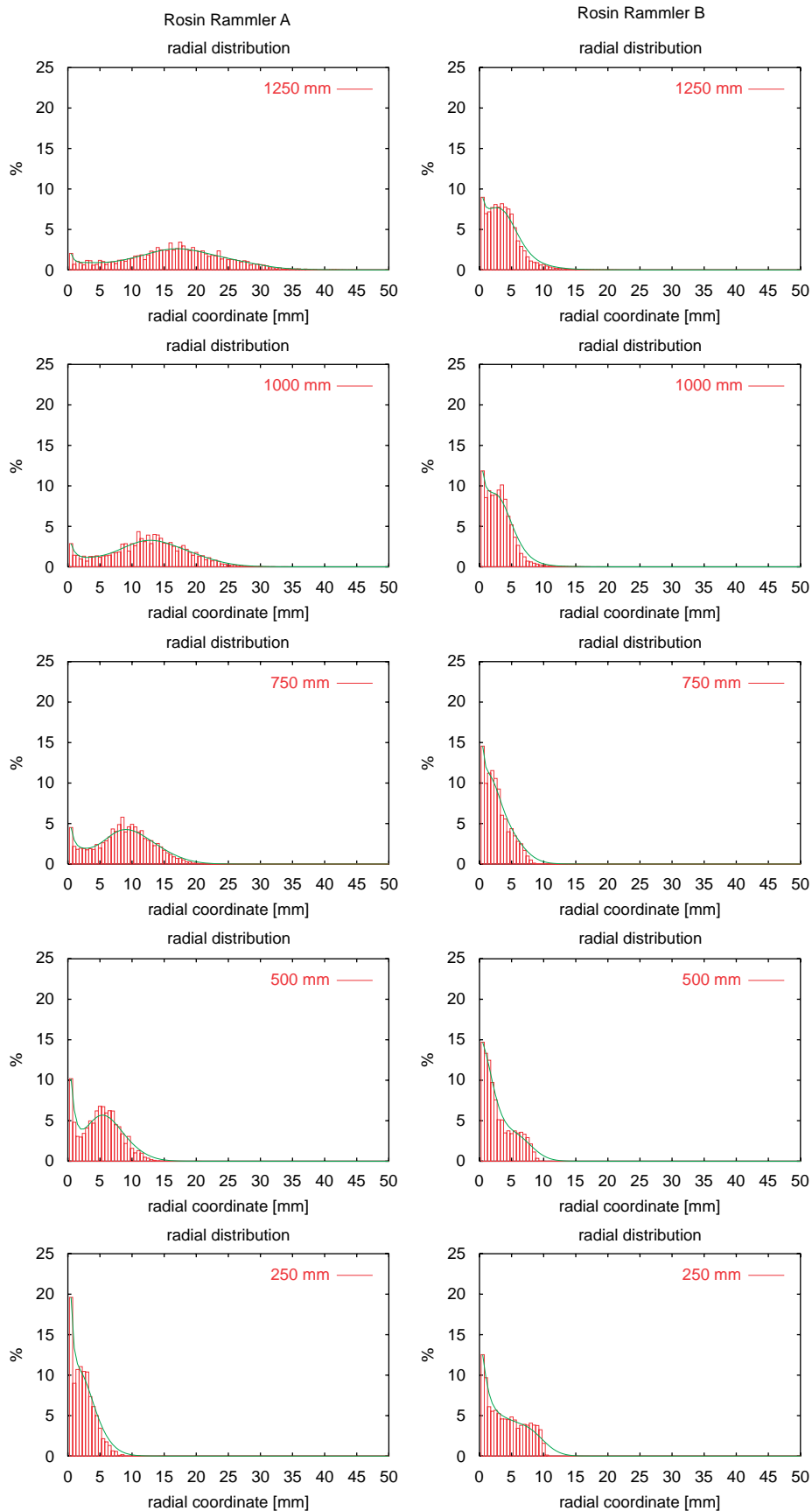


Fig. 7. Radial distribution of particles at five sections downstream the jet exit. Injector position $L2$. Rosin Rammler A and B.

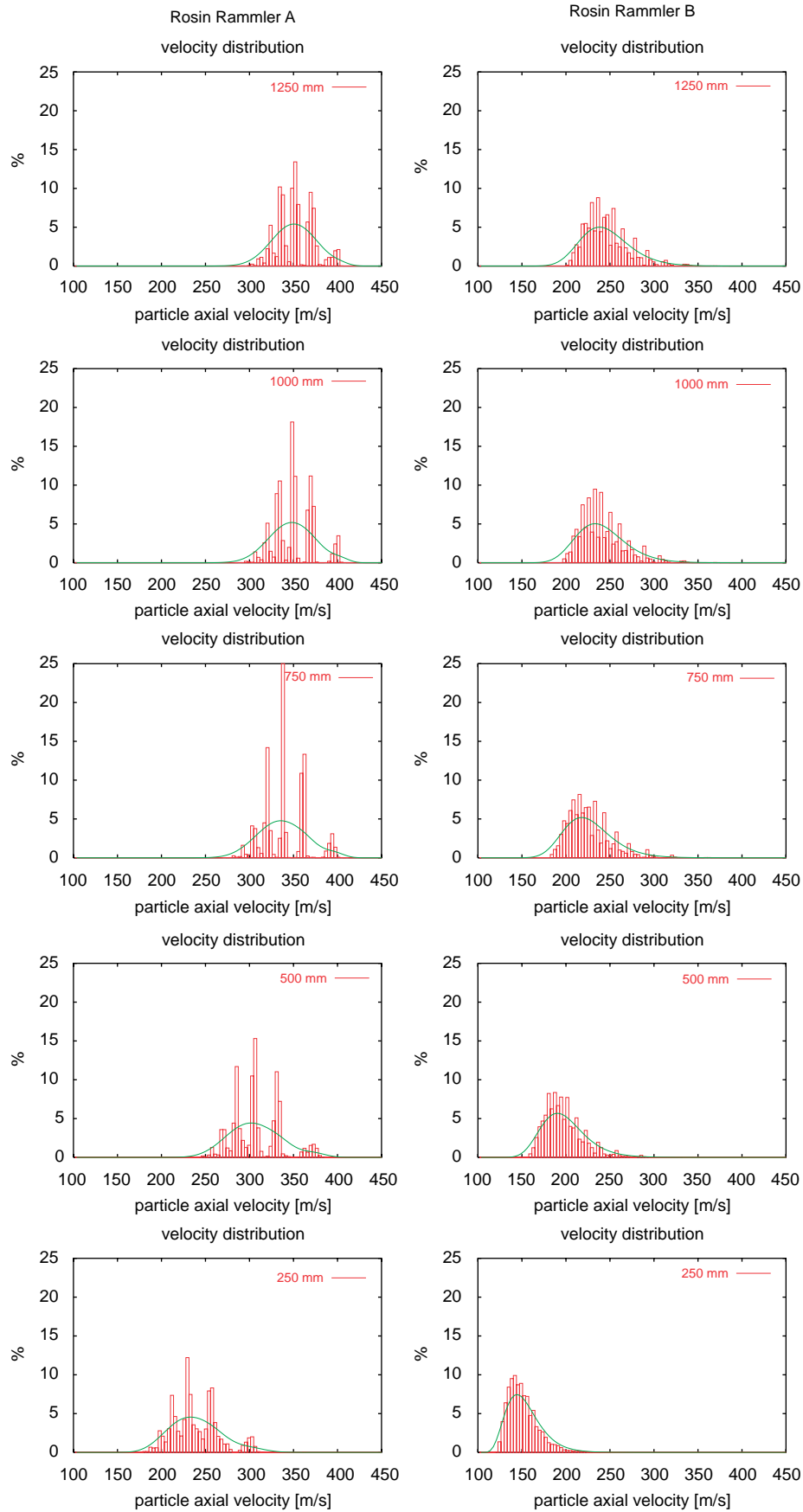


Fig. 8. Distribution of particle velocity at five sections downstream the jet exit. Injector position $L2$. Rosin Rammler A and B.

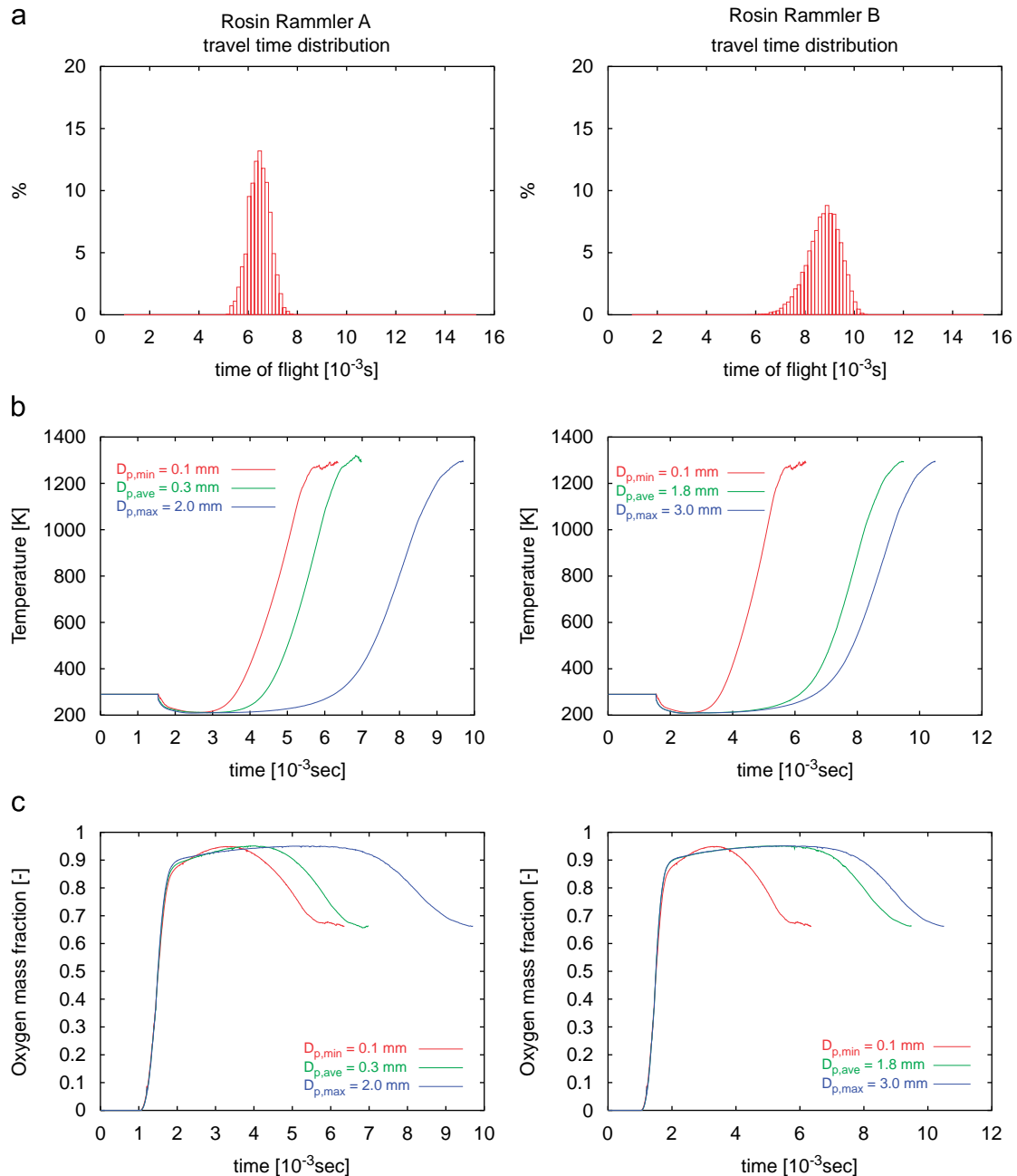


Fig. 9. Travel time distribution, thermal history and oxygen history of carbon particles for Rosin–Rammler distribution A: behaviour of particles with minimum, average and maximum diameter. Injector position $L2$.

table indicate that carbon particles spend very little time into the furnace and that larger average travel time corresponds to larger size particles.

Fig. 9(b) shows the thermal field sampled by particles from RR-A and RR-B distributions and injector position $L2$. Different size particles spread radially into different regions of the jet, sampling regions of the fluid which are at different temperatures. The temperature of the background fluid sampled by particle controls: (i) the amount of heat which can be transferred by convection contributing to particle heating; (ii) the rate of oxidation and (iii) the rate of devolatilization. Therefore,

thermal characteristics of the background environment should be reproduced precisely to compute reliable estimates of carbon injection yield. Here, they are evaluated from the statistics obtained from the Lagrangian particle tracking. Statistics are presented with reference to minimum, average and maximum diameter using red, green and blue lines, respectively, and discussed in relation with a value of temperature ($T = 500$ K) which fixes the onset of particle devolatilization for the quality of carbon analyzed in this work. Consider first results obtained for distribution RR-A. Due to their larger radial dispersion, minimum size particles sample, in a short time, regions of

Table 5
 Statistics of travel time distribution, temperature and oxygen mass fraction for RR-A and RR-B and all injector positions

	Injector position L1		Injector position L2	
	RR-A	RR-B	RR-A	RR-B
Travel time (s)				
Minimum	4.04×10^{-3}	4.33×10^{-3}	5.18×10^{-3}	5.61×10^{-3}
Mean	5.36×10^{-3}	7.11×10^{-3}	6.44×10^{-3}	8.69×10^{-3}
Maximum	7.18×10^{-3}	8.61×10^{-3}	8.32×10^{-3}	1.05×10^{-2}
Variance	4.58×10^{-4}	8.38×10^{-4}	4.27×10^{-4}	9.62×10^{-4}
Temperature (K)				
Minimum	220	220	220	220
Maximum	480	480	1350	1300
Time $T > 500$ K	0	0	$t > 4-7.2 \times 10^{-3}$ s	$t > 4-8 \times 10^{-3}$ s
Oxygen mass fraction				
$X_{O_2} < 0.1$	$t < 1.2 \times 10^{-3}$ s	$t < 1.2 \times 10^{-3}$ s	$t < 1.1 \times 10^{-3}$ s	$t < 1.2 \times 10^{-3}$ s
$X_{O_2} > 0.85$	$t > 1.7 \times 10^{-3}$ s	$t > 1.8 \times 10^{-3}$ s	$t > 1.8 \times 10^{-3}$ s	$t > 1.8 \times 10^{-3}$ s

the flow characterized by large temperature variations. Largest temperatures are found near the slag, at the end of their travel into the furnace. Average size particles move at a lower velocity in the furnace and take more time to sample the same regions of the flow; maximum size particles move into high temperature regions ($T \geq 500$ K) even more slowly (0.006 s after injection) and stay there for the last 0.002 s of their travel. Considering the green line representative of the average behaviour of the swarm, RR-A particles move into high temperature regions only during the last 0.001 s of their travel, i.e., a short time to produce significant heat transfer to the particles and carbon devolatilization. The situation is modified for distribution RR-B, for which the average diameter of particles is larger than in distribution RR-A. Particles stay in high temperature regions of the fluid ($T \geq 500$ K) for the last 0.002 s of their travel, like the larger particles in distribution RR-A. They have more time (yet, still very short) to exchange convective heat with the surrounding and radiative heat with the walls of the furnace and slag.

Fig. 9(c) shows the oxygen mass fraction seen by the particles as a function of time, calculated for distributions RR-A and RR-B and injector position L2. Statistics are presented again with reference to minimum, average and maximum diameter using red, green and blue lines, respectively. We observe that, as soon as particles are injected into the furnace ($t > 0.0015$ s), they move into an oxygen-rich environment. The mass fraction of oxygen is about 0.9 all along their travel. Differences observed between distributions RR-A and RR-B for sampled mass fraction of oxygen are negligible, whereas the residence time of particles changes significantly.

4.5. Coal devolatilization and oxidation in the particle-laden jet

4.5.1. Identification of conservative conditions for RNA analysis

The Lagrangian characterization of the reacting environment shows that: (i) smaller particles, which have the most favorable

surface-to-mass ratio to promote devolatilization and chemical reaction, spend the smallest time in the furnace; (ii) larger particles, which spend the largest time in the furnace, have the less favorable surface to mass ratio to promote devolatilization and chemical reaction. Therefore, independently from the particle diameter, carbon particle injection yield may remain high even if particles move across high temperature and high oxygen mass fraction regions.

Table 5 briefly summarizes detailed results from the numerical analysis which have been used to identify conservative conditions to run reactor network analysis for carbon particles in the EAF.

Consider first results obtained for injection distance L1. No particles reach the temperature levels (> 500 K) necessary for the onset of devolatilization and oxidation phenomena, independently of the size distribution. For this reason, devolatilization and combustion of particles will be not analysed further for injection position L1.

For injection distance L2, larger particles (distribution RR-B) are those spending more time in regions where the temperature is sufficiently high to start massive devolatilization and combustion. Nevertheless, the large diameter makes devolatilization and combustion less favorable than for smaller particles. Carbon consumption during the time of flight of particles is expected to be less important for size distribution RR-B than for size distribution RR-A. For this reason, devolatilization and combustion of particles from RR-B distribution will be not analysed further in this study.

The configuration which will be studied in detail using RNA is the EAF-RRA-L2, which represents a conservative case for the evaluation of carbon consumption—large time of flight for particles and maximum sampled temperature.

4.5.2. Verification of validity of initial assumptions

Lagrangian characterization of EAF environment has been obtained from particle tracking statistics assuming that: (i) the mass of each single particle is conserved; (ii) convective and radiative heat exchange do not contribute significantly to

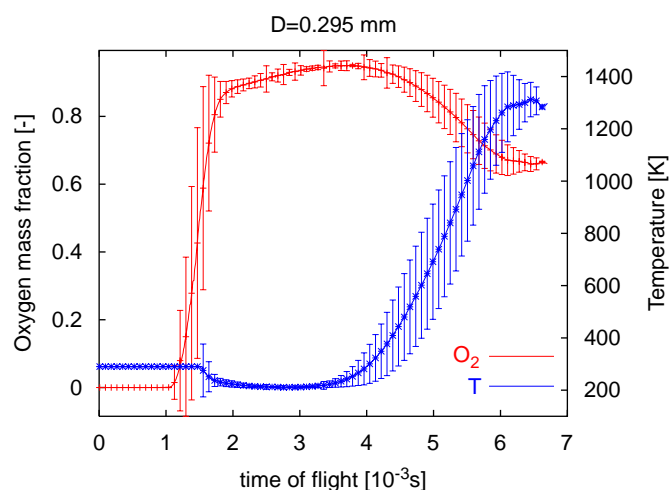


Fig. 10. Oxygen mass fraction and thermal history for injected carbon particles from CFD analysis. Injector position $L2$, $D_p = 0.2$ mm, i.e., average diameter of RR-A.

particle heating. Fig. 10 shows temperature and oxygen mass fraction sampled by average size particles. Error bars are used to indicate standard deviation of the variables as particles move inside the EAF. We performed preliminary RNA simulations to verify that assumptions (i) and (ii) do not introduce severe error in calculated Lagrangian statistics when the most critical operating conditions, corresponding to the smallest particles are considered. These particles are supposed to diffuse outside the centre line of the jet, being exposed to the most severe thermal gradients with respect to particles traveling in the center line of the jet. Furthermore, due to the most favorable ratio between surface exposed to heating and volume heat capacity, radiative effects are expected to be the most significant.

To assess the importance of particle heating from convective and radiative effects and the amount of devolatilization during the time of flight, we solved the mass and thermal balance equation for the smallest particle switching on and off the different terms in the mass and thermal balance. We used empirical correlation for convective heat transfer coefficient, literature data for coal emissivity and conventional modelling of coal devolatilization (SFOR and distributed activation energy model, DAEM). Parameters calculated considering the temperature time history reported in Fig. 10 (the worst case in terms of thermal treatment severity) (Biagini et al., 2004) are reported in Table 7. These values are exactly those reported in Pedersen et al. (1998). Since the initial char reactivity depends on coal properties, correlation between standard coal analysis and kinetic constants have been produced based on Hurt and Mitchell measurements (1992). While the initial char reactivity is specified from calibration procedures, the activation energy parameter is adjusted to match the predicted unburned carbon (UBC) emission to reported values for a single set of operating conditions.

A sensitivity analysis demonstrated that, for all the coal types investigated (anthracite, petrolcoke, and other high volatile coals): (i) particle heating by convection and radiation is

negligible and (ii) less than 0.5% of volatile matter is released during time of flight for low rank coals, less than 0.1% of volatile matter is lost for high rank coals.

4.5.3. Network of reactors

Results discussed in Section 4.4.1 indicate that the motion of carbon particles is confined in a reduced portion of the computational domain corresponding to the jet region. To assess the effect of complex chemistry on particle devolatilization and oxidation, this region can be modelled as a plug flow reactor (PFR) or, equivalently, as a series of perfectly mixed stirred tank reactors (STR). Since the critical parameters controlling oxidation and devolatilization are the thermal history and the oxygen mass fraction, we base on these quantities to identify the equivalent network of reactors to be used to perform the accurate calculations involving detailed chemistry. Preliminary calculations show that expected conversion for carbon is less than 1%. This datum is used to evaluate the number of STR necessary to simulate the performance of the PFR. Following Levenspiel (1972) the number of equal size (V_i), equal residence time (τ_i) reactors in series approximating a PFR characterized by a given volume (V) and residence time (τ) can be evaluated as

$$\frac{-\ln(1-x)}{[(1-x)^{-1/n} - 1] \cdot n} = 0.9999, \quad (11)$$

where, n is the number of STR and x is carbon conversion. The left-hand side of Eq. (11) is the ratio between the residence time necessary to achieve desired conversion as calculated for the PFR (τ_{PFR}) and the residence time for a series of n STR ($n\tau_{\text{STR}}$). The right-hand side, equal to 0.9999, is the confidence level, i.e., the approximation we consider acceptable for the unity ratio. We should remark here that a larger number of STR is necessary to simulate precisely a PFR characterized by a larger conversion. In the present case, assuming carbon conversion equal to 1% ($x = 0.01$). Eq. (11) indicates that 80 STR are sufficient to simulate the jet. Volume and residence time for each reactor are calculated considering the volume of the particle-laden jet and the particle travel time divided by the number of reactors. Specifically, according to the thermal profile shown in Fig. 10, 20 reactors are used to schematize the low temperature region of the jet (400–500 K) and 60 reactors are used to describe the region where the temperature increases steeply from 500 to 1400 K.

Each reactor is characterized by input and output streams. Input streams are assumed perfectly mixed at the inlet of each reactor. For the first reactor in the chain, input streams are oxygen, gases entrained from the furnace atmosphere and carbon particles; output are reacted streams and devolatilization/combustion products. Output becomes input for each subsequent reactor in the chain.

We performed preliminary simulation to evaluate the effect on carbon particle oxidation/devolatilization due to variation in chemical composition of the reacting environment. Specifically, we considered two extreme cases, corresponding to the gas compositions found at the begin and at the end of the net of reactors (see Table 6).

Considering a constant gaseous atmosphere corresponding to these two extreme cases, we found that changes in the chemical composition of the environment have negligible effects on carbon conversion. Therefore, the evolution of the jet atmosphere during the time of flight of carbon particles has no effect for the modelling of particle oxidation and a constant bulk mass fraction of oxygen (equal to 90%) was assumed for all the simulations.

4.5.4. Results on carbon devolatilization/oxidation

The preliminary analysis demonstrated that, for all the coals investigated (anthracite, petrolcoke and other high volatile coals): (i) less than 0.5% of volatile matter is released during time of flight for low rank coals (high volatile matter, sub-bituminous coals); (ii) less than 0.1% of volatile matter is lost for high rank coals (anthracite). This means that, in the conditions of the jet, devolatilization can be considered negligible.

Since the oxygen mass fraction is very high during the time of flight of coal particles (about 90%), oxidation phenomena are supposed to be more critical in terms of carbon consumption. In order to assess the behaviour of a wide range of coal types, characterized by different reactivities and physical properties, we considered two extreme cases:

- (1) *Case 1*: High volatile coal, a bituminous coal with reactivity similar to Petrolcoke and larger devolatilization, with the following characteristics: fixed carbon, 64.4%, volatile matter 27.6%, ash 8%;
- (2) *Case 2*: Anthracite, representing a low reactive coal as those typically used in siderurgic applications (properties are those in Table 3).

Table 7 summarises coals reactivities, evaluated as previously described.

Two cases were considered also for carbon particle size distributions. Specifically, we simulated by RNA: (i) distribution

Table 6

Gas composition in the jet for two extreme cases, corresponding to the gas compositions found at the begin and the end of the net of reactors

	O ₂ min	O ₂ max
O ₂ % vol	65.00	90.00
CO% vol	12.95	3.70
CO ₂ % vol	3.25	0.93
H ₂ % vol	5.71	1.63
H ₂ O% vol	2.45	0.70
N ₂ % vol	10.64	3.04

Table 7

Kinetic parameters for char oxidation

	High Volatile coal (C1)	Anthracite (C2)
A (kgC/(m ² s Pa ^{0.5}))	1.469565	3.14754
E (J/mol)	102,930.83	120,188.67

RR-A ($D_{ave} = 0.295$ mm) and (ii) distribution RR-C (larger average diameter, $D_{ave} = 0.48$ mm, spreading exponent $n = 1.52305$), representative of larger size carbon particles used in the industry.

Only configuration EAF-L2 was considered, since it allows the evaluation of carbon oxidation/devolatilization under conservative conditions.

The injection efficiency of carbon particles is a function of the carbon burnout, defined as the ratio between the oxidized carbon and the initial carbon content of char particles ($1 - C_{char}/C_{char0} = 1 - \%C_{burnout}$). The results are shown in Figs. 11 and 12. Fig. 11 shows the variation of surface temperature

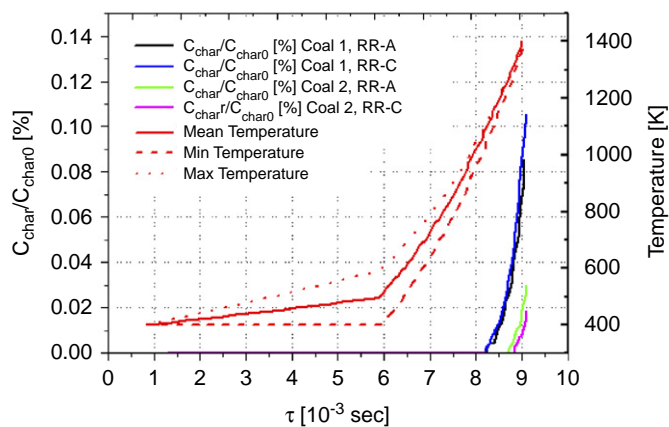


Fig. 11. Thermal history and char conversion for injected particles from reactor network analysis.

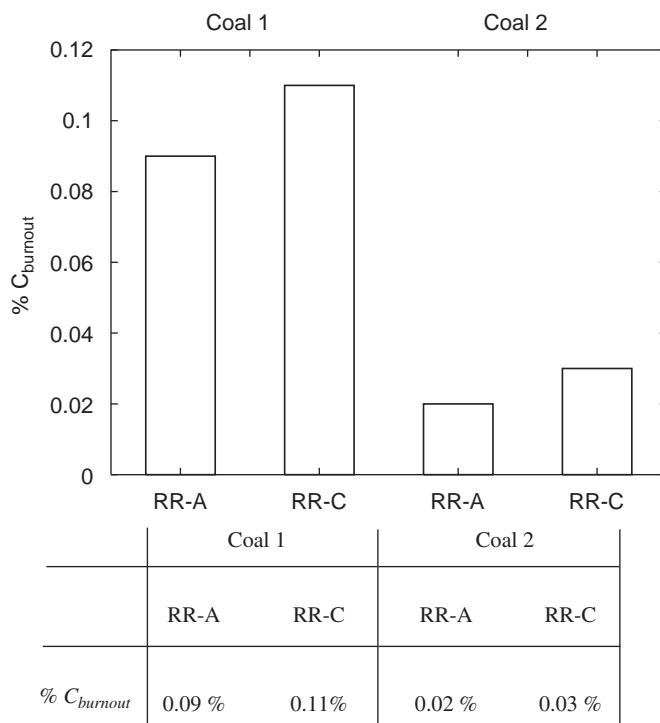


Fig. 12. Carbon burnout from RNA.

calculated for carbon particles belonging to distribution RR-A. The continuous line represents the mean value and dashed lines minimum and maximum value found for classes of different size. During the first 0.006 s of flight, the increase of particle temperature is reduced, since the only mechanisms contributing significantly to heat transfer are convection/radiation. No significant contribution is given by devolatilization and oxidation until the particle temperature rises up to 500 K. At this time, particles move into high temperature regions (nearer to the slag, temperature of the jet $T \geq 1000$ K), convective heat transfer is enhanced, particle heating is accelerated and devolatilization and combustion start to play a role in carbon consumption. Char oxidation/devolatilization takes place only in the last 2 ms of flight. Specifically, for the high volatile coal (C1), conversion becomes significant when the temperature of the carbon particle rises up to $T = 1000$ K. For Anthracite (C2), conversion becomes significant only at larger temperatures, $T \geq 1200$ K. We should remark here that no significant differences are observed for the different size distributions for high volatile coal, whereas small differences are observed for Anthracite. Specifically, a lower conversion is calculated for particles belonging to the larger size distribution (RR-C). Solid oxidation is practically unaffected by variations of oxygen mass fraction and temperature profile inside the particle-laden jet. In fact, particle temperature fluctuations in the jet are quite important in the first few milliseconds, where the levels are too low for oxidation to occur. Devolatilization and oxidation of coal particles starts only in the last milliseconds of flight, when temperature fluctuations are small with respect to the mean value. In the conditions of the jet (i.e., carbon type C2), devolatilization can be considered negligible whereas the oxidation process is dominated by thermal effects rather than by local composition. In the range of values produced by the entrainment (0.65–0.9 mass fraction), oxygen mass fraction has negligible influence on the rate of reaction (Hurt and Mitchell, 1992). The rate of reaction may change significantly with coal type, especially when high volatile coals are considered, and in this case particle size distribution effects can be appreciated. Even considering worst case conditions, calculated carbon burnout remains in the range 0.02–0.10%, indicating injection yield over 99%, i.e., a significant increase of EAF performances for systems equipped with the new concept injector.

5. Conclusion

In this paper, we present an original numerical procedure developed and adopted to characterize and quantify injection yields of a new-concept carbon particle injector designed for siderurgic applications. The injector exploits a supersonic jet of oxygen, coaxial to a low velocity air jet laden by carbon particles, to entrain and accelerate the particles toward the slag. Preliminary experimental tests performed on real furnaces indicate that a significant increase in carbon transport efficiency is obtained by the new configuration compared to the traditional configuration—i.e., high velocity, particle-laden air jet—, even if, during their travel inside the furnace, carbon particles are exposed to high temperatures and oxidizing conditions, which

could decrease significantly injection yields. The injection process is investigated numerically: (i) to analyse the factors contributing to improved performances; (ii) to identify the most critical configuration for the injector in the furnace and (iii) to obtain a conservative estimate of the injection yield of carbon particles, with the final aim of identifying strategies for injection device optimization. Numerical solution is regarded here as the only accurate prediction method since any experimental attempt to solve the problem is unrealistically expensive and extremely complex. We use state of the art techniques coupled to research tools to reproduce the evolution of the multiphase reacting system: specifically, complex chemistry models for carbon particles have been implemented (Reactor Network Analysis, RNA) on a simplified fluid dynamic model of the reacting environment identified by a detailed fluid dynamic analysis and Lagrangian statistics calculated for the dispersed phase. This methodology, which is beyond the capabilities of current softwares, offers a realistic picture of the multiphase reacting turbulent jet at a reasonable cost.

Results obtained in this work indicate that the positive effects on injection yields are produced by the supersonic injection which: (i) decreases drastically the residence time of carbon particles inside the furnace and (ii) modifies the hot reacting environment seen by carbon particles. Specifically, due to the reduced radial dispersion, devolatilization and oxidation of coal particles start only in the last millisecond of flight, a time too short to produce significant carbon consumption. Reaction rates for carbon oxidation process, which depend on oxygen mass fraction and temperature, are dominated by thermal effects and change significantly with coal type and particle size distribution. For the conditions tested in this work, variation of carbon burnout is bounded in the range 0.02–0.10%, indicating good performances of the new concept injector.

Acknowledgements

More s.r.l.[®] is gratefully acknowledged for support. We thank in particular Ing. Claudio Candusso and Mr. Daniele Tolazzi for valuable discussions on the technical problem.

References

- Badzioch, S., Hawksley, P.G.W., 1970. Kinetics of thermal decomposition of pulverized coal particles. *Industrial & Engineering Chemistry Process Design and Development* 9, 521–530.
- Balarac, G., Metais, O., 2005. The near field of coaxial jets: a numerical study. *Physics of Fluids* 17, 065102.
- Balarac, G., Si-Ameur, M., 2005. Mixing and coherent vortices in turbulent coaxial jets. *Comptes Rendus Mécanique* 333, 622–627.
- Baukal, C.E., 1998. *Oxygen-enhanced Combustion*. CRC Press, London.
- Biagini, E., Fantozzi, C., Tognotti, L., 2004. Characterisation of devolatilization of secondary fuels in different conditions. *Combustion Science and Technology* 176, 685–703.
- Campolo, M., Salvetti, M.V., Soldati, A., 2005. Mechanisms for microparticle dispersion in a jet in crossflow. *A.I.Ch.E. Journal* 51, 28–43.
- Carlson, D.J., Hoglund, R.F., 1964. Particle drag and heat transfer in rocket nozzles. *AIAA Journal* 2, 1980–1984.
- Chung, J.N., Troutt, T.R., 1988. Simulation of particle dispersion in an axisymmetric jet. *Journal of Fluid Mechanics* 186, 199–222.

- Coelho, L.M.R., Azevedo, J.T.L., Faravalli, T., Hesselmann, G., 2001. Integrated study of reburn technology by means of detailed chemical kinetics. CFD modelling and pilot scale testing. *IFRF Combustion Journal* 200108 ISSN 1562-479X.
- Crowe, C., Sommerfeld, M., Tsuji, Y., 1998. *Multiphase Flows With Droplets and Particles*. CRC Press, London.
- Dahal, M.D., Morris, P.J., 1997. Noise from supersonic coaxial jets. Part 1: mean flow prediction. *Journal of Sound & Vibration* 200, 643–663.
- Falcitelli, M., Tognotti, L., Pasini, S., 2002. An algorithm for extracting chemical reactor network models from CFD simulation of industrial combustion systems. *Combustion Science and Technology* 174, 27–42.
- Freund, J.B., Lele, S.K., Moin, P., 2000. Compressibility effects in a turbulent annular mixing layer. Part 1: Turbulence and growth rate. *Journal of Fluid Mechanics* 421, 229–267.
- Gosman, A.D., Ioannides, S.I., 1983. Aspects of computer simulation of liquid-fuelled combustors. *AIAA Journal Energy* 7 (6), 482–490.
- Graham, D.I., 1998. Improved Eddy interaction models with random length and time scales. *International Journal of Multiphase Flow* 24 (2), 335–345.
- Guo, D., Irons, G.A., 2003. Modelling of radiation intensity in an EAF. *Third International Conference on CFD in the Minerals and Process Industries. CSIRO*, Melbourne, Australia, 10–12 December 2003.
- Haider, A., Levenspiel, O., 1989. Drag coefficient and terminal velocity of spherical and non spherical particles. *Powder Technology* 58, 63–70.
- Hurt, R.H., Mitchell, R.E., 1992. Unified high-temperature char combustion kinetics for a suite of coals of various rank. In: 24th Symposium (International) on Combustion, 1243–1250.
- Levenspiel, O., 1972. *Chemical Reaction Engineering*. Wiley International Edition.
- Li, Y., Fruehan, R.J., 2003. Computational fluid dynamics simulation of postcombustion in the electric arc furnace. *Metallurgical and Materials Transactions B* 34, 333–343.
- Loth, E., 2000. Numerical approaches for motion of dispersed particles, droplets and bubbles. *Progress in Energy and Combustion Science* 26, 161–223.
- Magnussen, B.F., Hjertager, B.W., 1981. On the structure of turbulence and a generalised eddy dissipation concept for chemical reaction in turbulent flow. 19th AIAA Aerospace Meeting, St. Louis, USA.
- Marchisio, D.L., Barresi, A.A., 2003. CFD simulation of mixing and reaction: the relevance of the micro-mixing model. *Chemical Engineering Science* 58, 3579–3587.
- Maxey, M.R., Riley, J.J., 1983. Equation of motion for a small rigid sphere in a nonuniform flow. *Physics of Fluids* 26, 883–889.
- Niksa, S., Liu, G.S., 2002. Incorporating detailed reaction mechanisms into simulations of coal-nitrogen conversion in p.f. flames. *Fuel* 81, 2371–2385.
- Pallares, J., Arauzo, I., Diez, L.I., 2005. Numerical prediction of unburned carbon levels in large pulverized coal utility boilers. *Fuel* 84, 2364–2371.
- Pantano, C., Sarkar, S., 2002. A study of compressibility effects in the high speed turbulent shear layer using direct numerical simulation. *Journal of Fluid Mechanics* 451, 329–371.
- Patankar, S.V., Spalding, D.B., 1972. A calculation procedure for heat and mass transfer in three dimensional parabolic flows. *International Journal of Heat and Mass Transfer* 15, 1787–1806.
- Pedersen, L.S., Glarborg, P., Dam-Johansen, K., Hepburn, P.W., Hesselmann, G., 1998. A chemical engineering model for predicting NO emissions and burnout from pulverised coal flames. *Combustion Science and Technology* 132, 251–314.
- Please, C.P., McGuinness, M.J., McElwain, D.L.S., 2003. Approximations to the distributed activation energy model for the pyrolysis of coal. *Combustion and Flame* 133, 107–117.
- Ranzi, E., Dente, M., Goldaniga, A., Bozzano, G., Faravelli, T., 2001. Lumping procedures in detailed kinetic modeling of gasification, pyrolysis, partial oxidation and combustion of hydrocarbon mixtures. *Progress in Energy and Combustion Science* 27, 99–139.
- Rehab, H., Villermaux, E., Hopfinger, E.J., 1997. Flow regimes of large-velocity-ratio coaxial jets. *Journal of Fluid Mechanics* 345, 357–381.
- Sarkar, S., Erlebacher, G., Hussaini, M.Y., Kreiss, H.O., 1991. The analysis and modeling of dilatational terms in compressible turbulence. *Journal of Fluid Mechanics* 227, 473–493.
- Urban, W.D., Mungal, M.G., 2001. Planar velocity measurements in compressible mixing layers. *Journal of Fluid Mechanics* 431, 189–222.
- Villermaux, E., Rehab, H., 2000. Mixing in coaxial jets. *Journal of Fluid Mechanics* 425, 161–185.
- Yin, C.G., Rosendahl, L., Kaer, S.K., Condra, T.J., 2004. Use of numerical modeling in design for co-firing biomass in wall-fired burners. *Chemical Engineering Science* 59, 3281–3292.